Local Air-Sea Interactions at Ocean Mesoscale in Western Boundary Currents

Ehud Strobach[1], Patrice Klein[2], Andrea Molod[3], Abdullah A. Fahad[4], Atanas Trayanov[5], Dimitris Menemenlis[6], and Hector S Torres[6]

[1]Agricultural Research Organization
[2]Jet Propulsion Laboratory, California Institute of Technology - CNRS
[3]Goddard Space Flight Center(NASA)
[4]University of Maryland
[5]Science Applications International Corporation (United States)
[6]Jet Propulsion Laboratory, California Institute of Technology

November 21, 2022

Abstract

We present results from a new, global, high-resolution (~4-km for ocean and ~7-km for atmosphere) realistic earth system simulation. This simulation allows us to examine aspects of small-scale air-sea interaction beyond what previous studies have reported. Our study focuses on recurring intermittent wind events in the Gulf Stream region. These events induce local air-sea heat fluxes above Sea Surface Temperature (SST) anomalies with horizontal scales smaller than 500-km. In particular, strong latent heat bursts above warm SST anomalies are observed during these wind events. We show that such wind events are associated with a secondary circulation that acts to fuel the latent heat bursts by transferring dry air and momentum down to the surface. The intensity of this secondary circulation is related to the strength of small-scale SST fronts that border SST anomalies. The study of such phenomena requires high-resolution in both the atmospheric and oceanic components of the model.

Local Air-Sea Interactions at Ocean mesoscale in Western Boundary Currents

Ehud Strobach[1], Patrice Klein[2,3], Andrea Molod[4], Abdullah A. Fahad[4,7], Atanas Trayanov[4,5], Dimitris Menemenlis[6], Hector Torres[6]

[1]Agricultural Research Organization, Israel
[2]G.P.S. Division, California Institute of Technology, Pasadena, CA, US
[3]Laboratoire de Météorologie dynamique, Ecole Normale Supérieure, France
[4]NASA, Goddard Space Flight Center, MD, US
[5]Science Systems and Applications Inc., MD, US
[6]Jet Propulsion Laboratory, California Institute of Technology, Pasadena, CA, US
[7]ESSIC, University of Maryland, College Park, MD, US

Key Points:

- Strong turbulent flux discontinuities observed at ocean fronts suggest the importance of small scales for air-sea interactions
- Intermittent large-scale winds together with mesoscale SST variations trigger secondary circulations in the atmospheric boundary layer
- Air-sea interactions are explored under a wider range of periods and wind speeds than previously examined

Corresponding author: Ehud Strobach, `udist@volcani.agri.gov.il`

Abstract

We present results from a new, global, high-resolution (∼4-km for ocean and ∼7-km for atmosphere) realistic earth system simulation. This simulation allows us to examine aspects of small-scale air-sea interaction beyond what previous studies have reported. Our study focuses on recurring intermittent wind events in the Gulf Stream region. These events induce local air-sea heat fluxes above Sea Surface Temperature (SST) anomalies with horizontal scales smaller than 500-km. In particular, strong latent heat bursts above warm SST anomalies are observed during these wind events. We show that such wind events are associated with a secondary circulation that acts to fuel the latent heat bursts by transferring dry air and momentum down to the surface. The intensity of this secondary circulation is related to the strength of small-scale SST fronts that border SST anomalies. The study of such phenomena requires high-resolution in both the atmospheric and oceanic components of the model.

Plain Language Summary

We explore the atmospheric circulation above Sea Surface Temperature (SST) anomalies of less than 500 km-scale using a new, global, coupled ocean-atmosphere simulation performed at high horizontal resolution and integrated for three months. Our study focuses on intermittent wind events in the Gulf Stream region and the resulting local air-sea heat fluxes above warm SST anomalies: a strong latent heat burst above these SST anomalies is observed during the intermittent wind events. Furthermore, during these events, a secondary circulation develops up to altitudes of 2000 m above warm SST anomalies, which results in sinking of warm and dry air and air momentum from upper levels down to the sea-surface. Such secondary circulation is triggered by the strong wind stress divergences that develop above small-scale SST fronts bordering the SST anomalies. The consequence is an increase of latent heat fluxes above SST anomalies.

1 Introduction

The physical climate system is fundamentally linked to the mechanisms that transport heat between the ocean interior and the upper troposphere across the air-sea interface. One major gateway for this transport is associated with the action of mesoscale sea surface temperature (SST) anomalies with typical spatial scales of 10– 500 km (Griffies et al., 2015; Su et al., 2018, 2020). These SST anomalies, reaching magnitudes of $2.5°C$-$3°C$ and bordered by small-scale SST fronts, are driven by the baroclinic instability in the ocean interior that produces mesoscale eddies, in particular in Western Boundary Currents (WBCs) and in the Antarctic Circumpolar Current (ACC) (Chelton et al., 2011; Klein et al., 2019). In these regions, mesoscale eddies are thought to explain most of the upward vertical heat transport in the global ocean, up to $7PW$ close to the surface, leading to a cooling of the ocean interior and a warming of surface layers (Su et al., 2018, 2020). Such transport is balanced by the downward heat transport explained by the large-scale wind-driven circulation and small-scale diffusive processes (Griffies et al., 2015; Rackow et al., 2019).

Air masses passing over mesoscale SST anomalies are forced out of equilibrium as they encounter large differences between SST and air temperature. This is true only for SST anomalies with scales smaller than 500 km (Small et al., 2019), since at these scales air masses do not have enough time to adjust to SST changes. The resulting latent heat flux (LHF) anomalies, strongly intensified over warm SST anomalies, can exceed monthly magnitudes of 60 Wm^{-2} (Small et al., 2019), meaning that the ocean at mesoscale heats the atmosphere. WBCs and the ACC can be colocated with the atmospheric storm tracks, and this suggests a possible impact on the global atmospheric circulation through the intensified air-sea heat fluxes at the ocean mesoscale. Foussard, Lapeyre, and Riwal (2019), using an idealized model, showed that the latent heat release driven by mesoscale SST anomalies leads to a poleward shift of atmospheric storm tracks by up to 1000 km. Ma et al. (2015) and Liu et al. (2021) pointed out that, through these processes, mesoscale eddies in the Kuroshio Extension have a remote influence on the rainfall over the West Coast of the U.S..

Recent studies with idealized atmospheric models at high spatial resolution (Wenegrat & Arthur, 2018; Sullivan et al., 2020) emphasize that intermittent wind blowing over warm mesoscale SST anomalies can lead to more intensified air-sea exchange when these anomalies are bordered by strong SST fronts at smaller scales (submesoscale). The mechanism involved is a secondary circulation in the atmospheric planetary boundary layer (APBL) triggered by these fronts.

All the previous studies on ocean-mesoscale air-sea interactions were conducted using either limited observations and moderate horizontal resolution, moderate resolution models, or high-resolution idealized 2D dry-atmosphere models, and the majority of these analyzed monthly mean behavior. These studies therefore have limited scope in terms of realism, temporal resolution, and range of wind speeds. The present study revisits the impact of these strong fronts on the air-sea exchange using a realistic global coupled ocean-atmosphere model with very high spatial resolution and sub-hourly output, which allows us to explore a wider range of periods and wind speeds in a realistic simulation that includes the effects of latent heating. This new simulation will allow us to fill-in gaps from the previous observational or simplified-model studies. The next section describes the numerical coupled model. Section 3 presents and discusses the results. A conclusion is offered in the last section.

2 Model Description and Experimental setup

The coupled model used in this study is the Goddard Earth Observing System (GEOS) infrastructure and atmospheric model coupled to the the Massachusetts Institute of Technology general circulation ocean model (MITgcm). A description of the main features of the coupled model (hereafter called GEOS-MITgcm) can be found in (Strobach et al., 2020). The model simulation was initialized on 21 March, 2012 using ocean initial conditions from a similar resolution ocean only simulation (Su et al., 2018) and atmospheric initial conditions from an atmosphere-only experiment (Strobach et al., 2020). The atmospheric model was configured to run with nominal horizontal grid spacing of 6 km and 72 vertical levels, while the ocean was configured to run with nominal horizontal grid spacing of 6 km and 90 vertical levels. The time step for the atmosphere, the ocean, and the communication between them is 45 seconds. The results shown in this study are based on the 75 day segment of the simulation from April 22 to Jun 6.

3 Results

Our study focuses on the Gulf Stream (GS) region that hosts energetic mesoscale eddies. An example of the impact of mesoscale SST anomalies on the local atmospheric weather is shown in Figures 1a,b which emphasize the strong correspondence between the total turbulent heat fluxes at the sea surface (panel a) and the SST anomalies (panel b). Mesoscale SST anomalies are bordered by submesoscale SST fronts, with a $\sim$ 10 km width and an amplitude of up to $\sim$ 0.5°C per km (Figure 1b). Patterns of large turbulent heat fluxes, with magnitudes up to 500 W.m^{-2} (Figure 1a) display a strong discontinuity just above SST fronts. To understand how submesoscale SST fronts impact the interactions between the ocean and the atmosphere, we first analyze the relationship between these fronts and the wind stress curl and divergence. Next we describe the secondary circulation within the atmosphere in response to mesoscale and submesocale SST structures. Finally, we analyse the time and spatial scales involved in the resulting air-sea heat exchanges.

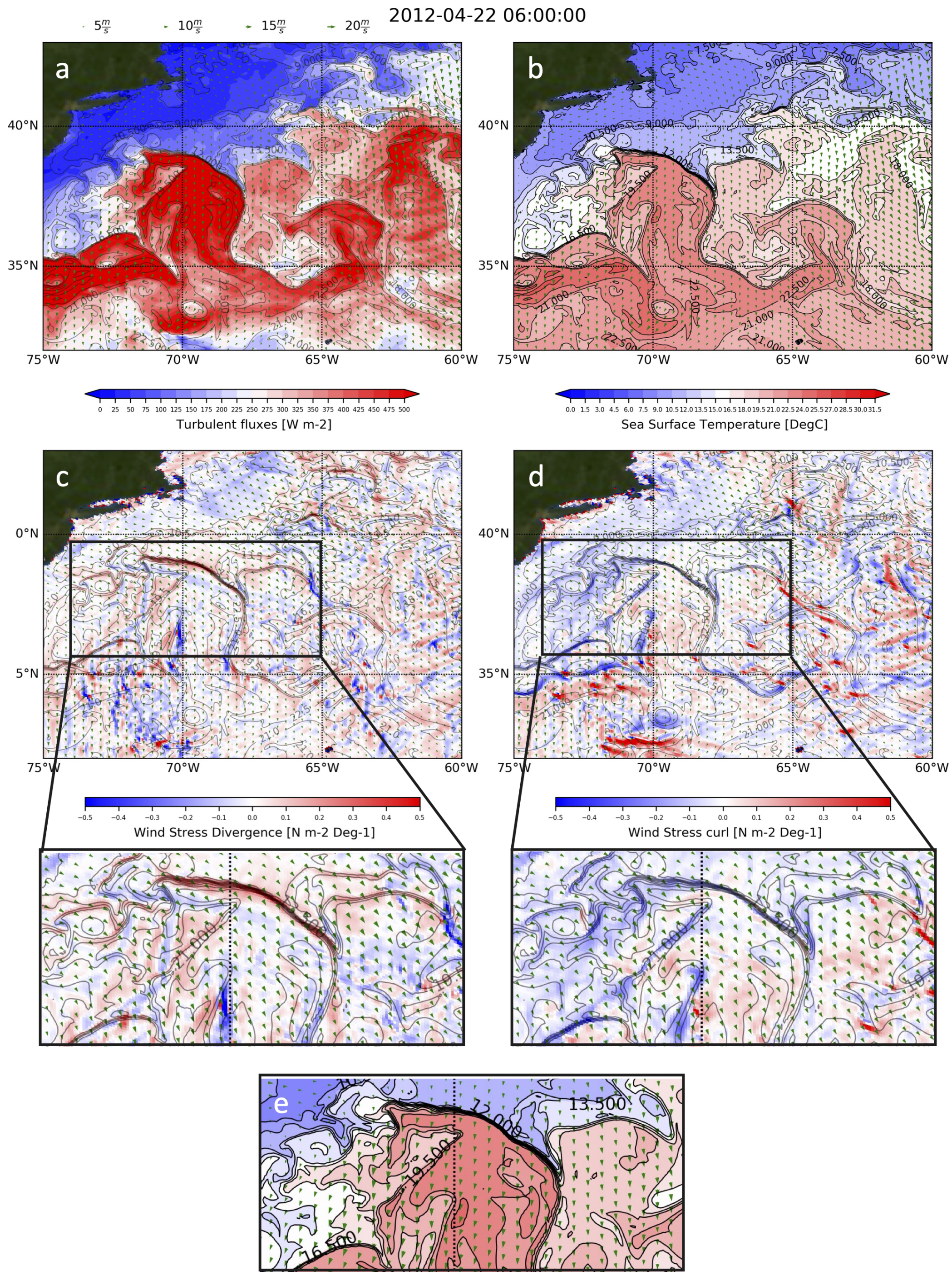

Figure 1. An overview over the Gulf Stream domain. **a, b** A snapshot of surface winds vectors overlaid on Turbulent fluxes (a) and SST (b) in the Gulf Stream region. **c, d, e** 24 hour mean (6AM to 6AM) surface winds (arrows) overlaid on wind stress divergence (c) and curl (d), and expended view over the SST front region (e).

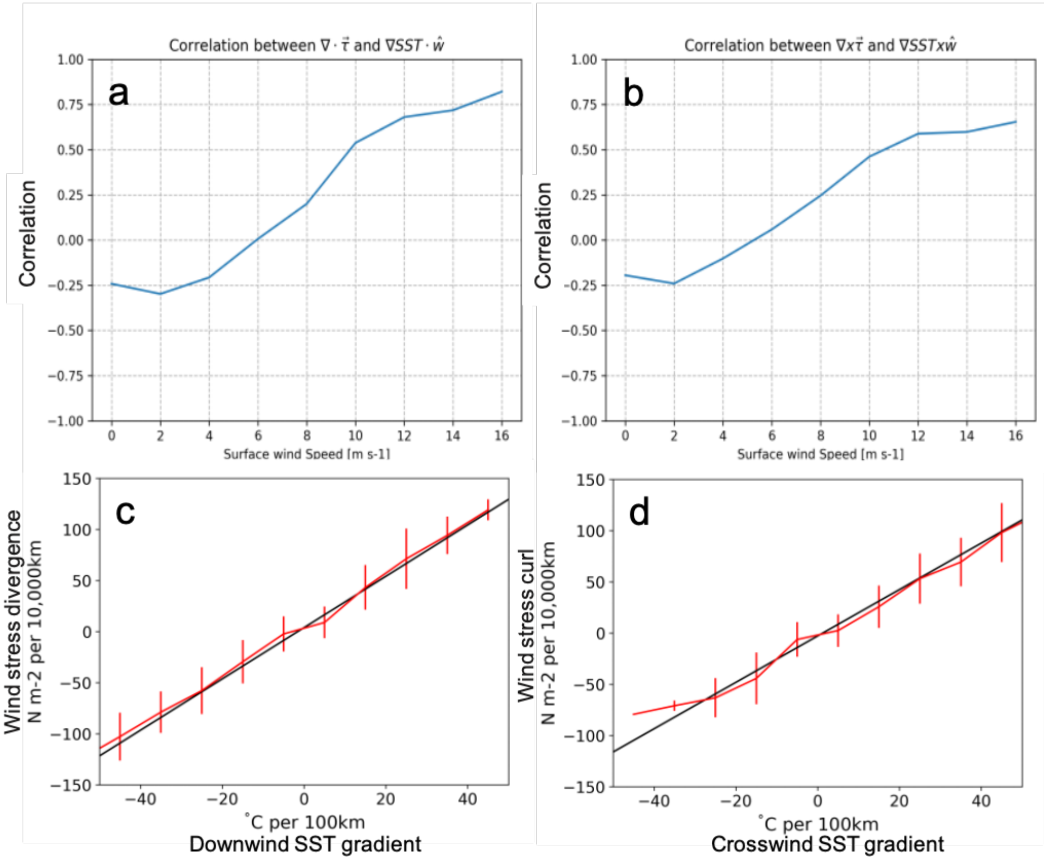

Figure 2. Correlation between the wind stress divergence and downwind SST gradient (**a**), and between the wind stress curl and crosswind SST gradient (**b**) as a function of the background surface winds. (**c**) and (**d**): binned scatter plots at high background wind conditions with error bars representing one standard deviation of the bin's scatter.

3.1 Wind stress curl and divergence in response to submesoscale SST fronts

Following previous studies (Lindzen & Nigam, 1987; Chelton et al., 2001; O'Neill et al., 2003), we first analyze the local atmospheric wind response to submesoscale SST fronts ($\sim$ 10 km) in terms of the wind stress curl/divergence. The snapshots on Figures 1c,d reveal that, with a strong background wind blowing from the northwest, the anomalies of local wind stress curl and divergence have a width close to that of SST fronts, and reach magnitudes up to $\sim$ 50 N.m^{-2} per 10,000 km ($\sim$ 0.5 N.m^{-2} per Deg^{-1}). Such magnitudes are two orders larger than what is traditional seen in monthly-mean lower-resolution observations (Chelton et al., 2004), and ten to fifteen times larger than results from coupled simulations with a resolution of only 25 km in the atmosphere (Putrasahan et al., 2013; Takatama & Schneider, 2017; Foussard, Lapeyre, & Plougonven, 2019). The background wind speed and direction vary at time scales of one to several hours. A movie (not shown) reveals that the resulting local wind stress curl/divergence adjusts almost instantaneously. This emphasizes how the strength of SST fronts and time intermittent large-scale wind conditions impact the local wind response at submesoscale.

Figures 2a and b show the correlation between the windstress curl/divergence and the SST gradients (crosswind and downwind) as a function of the background surface

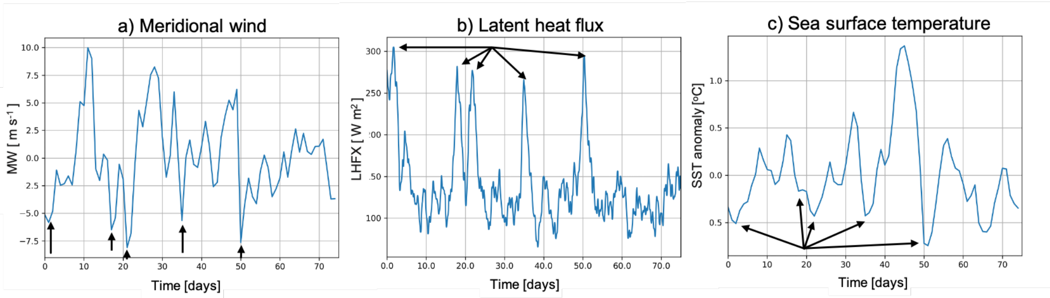

Figure 3. Time series of domain average latent heat flux (a), meridional wind (b), and SST (c). Black arrows represent the five latent heat burst events.

wind speed. Correlations are positive and high with strong winds as expected from previous studies (Chelton et al., 2001; O'Neill et al., 2003; Chelton et al., 2004; Foussard, Lapeyre, & Plougonven, 2019) but quickly decrease and flip sign for wind speeds lower than 5 m.s^{-1}. The correlation patterns are consistent with Foussard, Lapeyre, and Plougonven (2019) who found that, with strong background winds, the wind stress curl/divergence correlate well with SST gradients, whereas with weak background winds they correlate with the Laplacian of the SST (as advocated by Lindzen and Nigam (1987)). In addition, the flip in sign is explained by the large magnitude of the submesoscale SST fronts. Indeed, such strong SST fronts are known to be ageostrophic, leading to an opposite sign of the SST Laplacian and the SST gradient, as explained in Thomas et al. (2008).

Figures 2c and 2d further reveal the expected relationship between wind stress curl (and divergence) and SST gradients in the high wind speed regime (Chelton et al., 2004; Putrasahan et al., 2013; Takatama & Schneider, 2017). The slope is positive for both the wind stress curl and divergence indicating that the correlation with the SST gradient is mostly explained by moderate or strong winds. Values of these slopes are very close to those found in previous studies using coupled simulations with lower resolution (Putrasahan et al., 2013; Takatama & Schneider, 2017; Foussard, Lapeyre, & Plougonven, 2019). However, the magnitudes of the windstress curl/divergence exceed ~ 1 N.m^{-2} per Deg^{-1}, which is again more than ten to fifteen times larger than found in earlier studies. Such result emphasizes the significant impact of strong submesoscale SST fronts on the local wind response over three months. As shown by Chelton et al. (2004), the relationship between the windstress curl/divergence and SST gradients means that the local wind response over mesoscale eddies is intensified over warm eddies and decreased over cold eddies. The next section further explores the mechanisms involved in the local wind response at the mesoscale when such large values of the windstress curl/divergence are present.

3.2 Characteristics of the local atmospheric response to SST anomalies at meso- and submeso-scales

Over the GS region, atmospheric weather includes numerous frontal synoptic systems characterized by cold air outbreaks off the east coast of the United States. These outbreaks typically last for 1-5 days and are associated with strong intermittent southward winds as illustrated in Figure 3a. Such intermittent wind events are intimately associated with strong LHF at the air-sea interface above warm SSTs that reach magnitudes of up to 300 W.m^{-2} when averaged over the domain of (Figure 1). These fluxes lead to an SST decrease of up to 0.5°C (Figure 3c), which is much smaller than the magnitude of mesoscale SST anomalies.

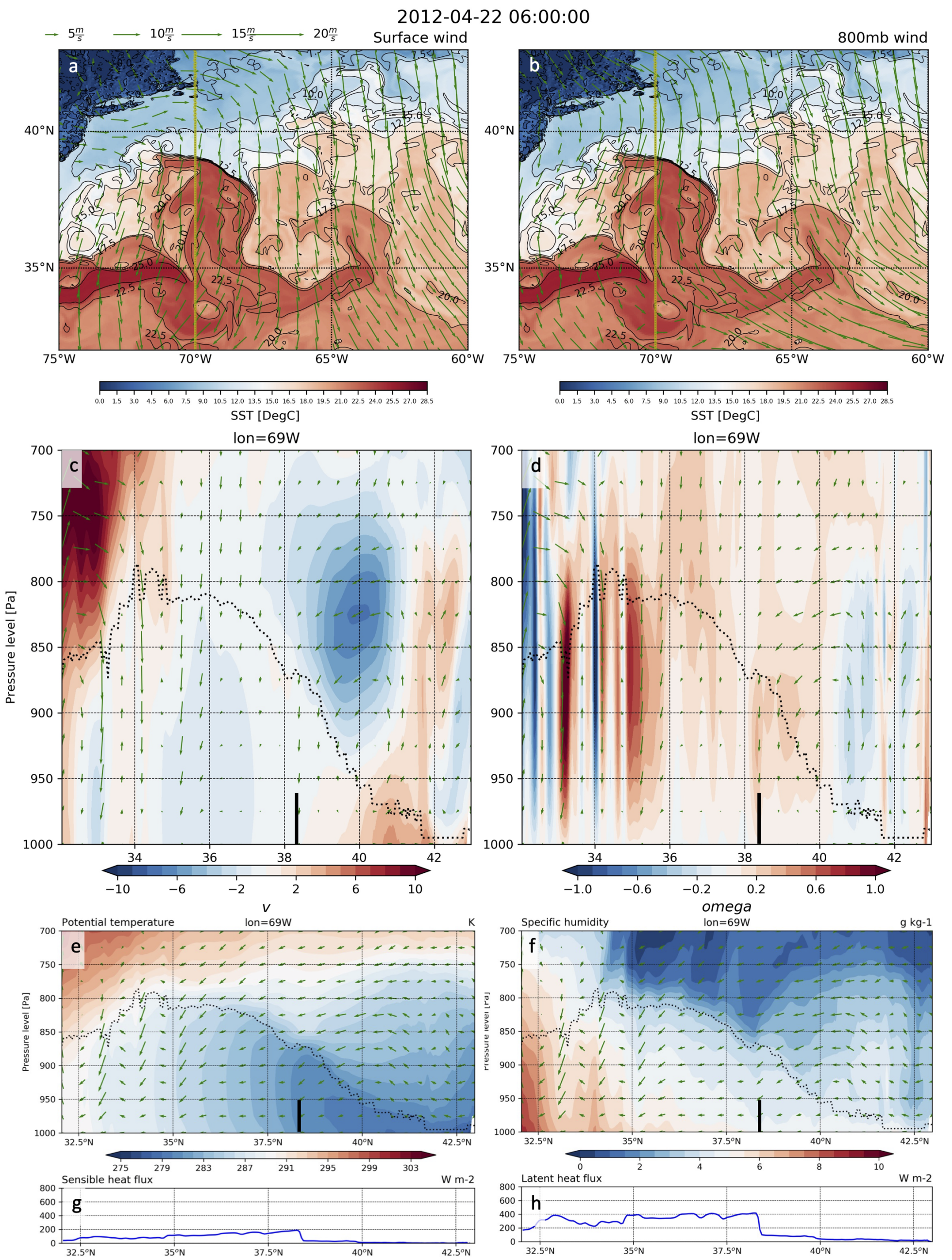

Figure 4. **a, b** A snapshot of surface (a) and 800mb (b) winds for the first latent heat burst event overlaid on SST. **c, d** Vertical cross sections (lon=69) of meridional wind anomaly with respect to the mean horizontal flow (c) and omega (d). Dashed black line depict the pressure level of the APBL. black vertical lines denote the location of the SST front. Green arrows represent the wind vector normalized to the panel aspect ratio. **e, f** Potential temperature in shading, pressure level at the top of the PBL in dotted black lines, and wind arrows. **g, h** Turbulent sensible and latent heat fluxes.

We observed five strong wind events during our simulation period (see arrows on Figure 3), each one associated with a strong latent heat burst. Understanding the mechanisms that drive these LHF bursts requires a case by case study as the interactions are highly non-linear and front locations and strengths vary. In the rest of this section, we focus only on the first event, having in mind that the driving mechanisms are very similar for the other four. As illustrated in Figure 4, cold air at the surface crosses submesoscale SST fronts and quickly accelerates over warm SST anomalies, as seen by the increase in the arrow size south of 40°N near the SST maximum (Figure 4a). Above the APBL, the air-mass accelerates before the front (Figure 4b), as can be seen by the increase in arrow size north of 40°N. In these weather conditions, the APBL height over warm SST anomalies smoothly increases from $\sim$ 200 m up to $\sim$ 2000 m, as depicted in Figures 4c, d (dotted lines). The lower APBL height north of the front reflects in part the sinking motion in the atmosphere associated with the secondary circulation (see the green arrows in Figures 4c, d). Also in Figure 4c, d, above the APBL at the transition region, the strong meridional wind increase before the front (blue blob in Figure 4) is associated with downward motion (positive omega). At the surface the opposite pattern is found – wind slowdown before the front and speedup after the front. The horizontal wind anomalies are associated with downward motions as confirmed by Figure 4c,d. This is a consequence of the strong wind stress divergence triggered by the SST front, whose impact reaches an altitude of up to 2500 m. Thus, in addition to the main surface wind that brings dry and cold air from the cold side of the front to the warm side, the secondary circulation results in sinking of warm and dry air from the upper levels down to the surface over warm SST (Figure 4e,f). This maintains the LHF and SHF discontinuities just after the SST front (Figure 4g,h).

Figure 5 illustrates these mechanisms schematically. In the absence of an SST front, a cold air mass moving from the right will 'dig' underneath warm air and push it upward (Figure 5a). In the SST front region, without the entrance of a cold air mass, a discontinuity in the APBL will be maintained. Higher APBL will form above warmer SST due to higher mixing (Figure 5b). When a cold air-mass approaches an SST front (Figure 5c), the warmer air at the surface will be pushed upward but, combined with mixing, will sink back bringing warmer but dryer air to the surface. The secondary circulation reported in this section is similar to that described in previous studies (Kilpatrick et al., 2014; Wenegrat & Arthur, 2018; Sullivan et al., 2020). However the discrepancy between LHF and SHF mentioned above points to a specific impact of moist processes on the atmospheric response to submesoscale SST fronts. This impact has not been reported in these previous studies since they only considered a dry atmosphere.

3.3 Amplification of LHF anomalies in a fully coupled system

Energetic wind and SST anomalies are usually characterized by different time and space scales; wind anomalies are dominated by spatial scales larger than 500 km and time scales smaller than 5 days, while SST anomalies are dominated by scales smaller than 500 km and time scales larger than five days (see spectra in the supplemental material). The air-sea coupling causes SST anomalies to have an imprint on wind anomalies and vice-versa. As emphasized in the preceding section, mesoscale SST anomalies drive a local wind response at the same scales (due to the secondary circulation), with local wind speed increased (decreased) over warm (cold) SST anomalies. Similarly, large-scale time-intermittent wind stress anomalies are known to impact SST at the same scale (strong winds mix the upper ocean layer leading to negative large-scale SST anomalies). In this section we examine the consequences of these coupling mechanisms on LHF anomalies. For that purpose, LHF (Q_E) is expressed in terms of mechanical and thermal components

$$Q_E = \rho \cdot L_V \cdot CQ \cdot \Delta q \tag{1}$$

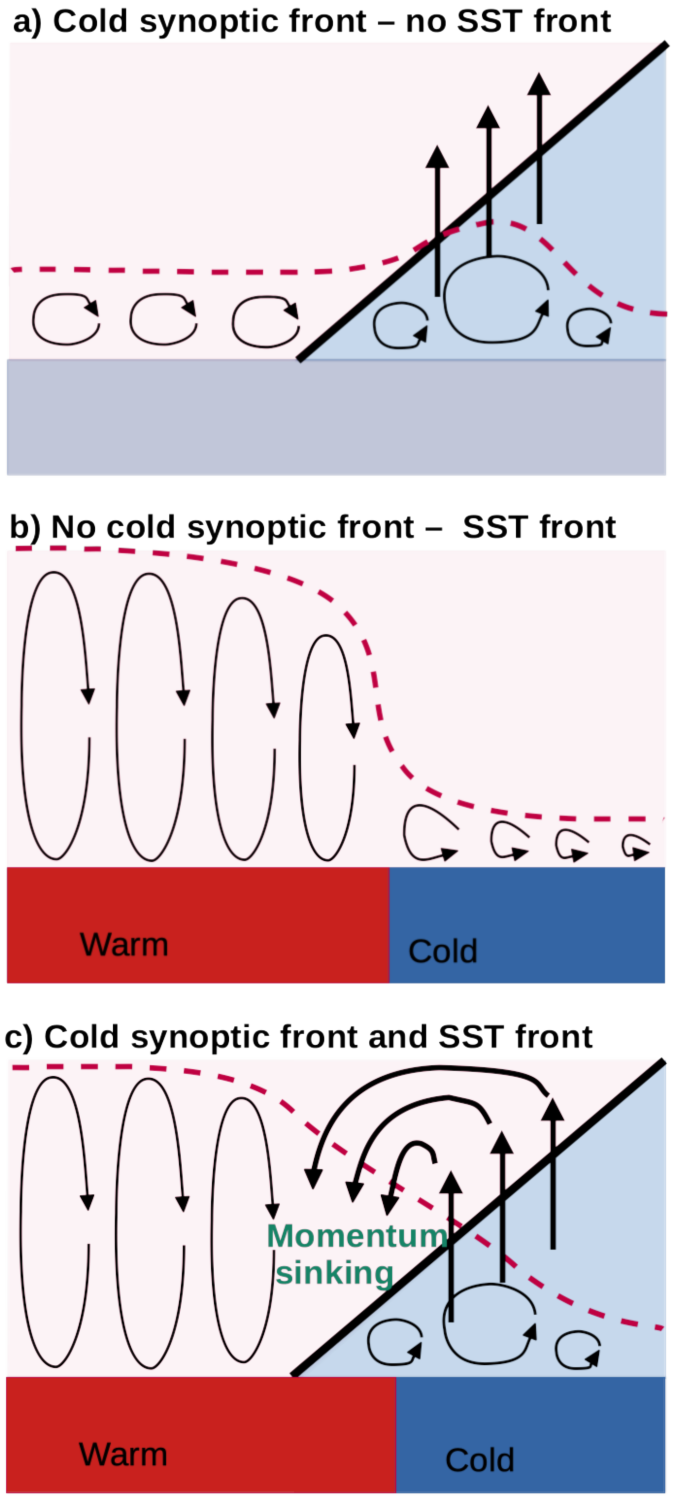

Figure 5. (a) Cold air-mass approaches an SST front, the warmer air at the surface is pushed upward. (b) Higher APBL forms above warmer SST due to higher mixing at no front conditions. (c) Cold air-mass approaches to the front and produces momentum sinking above the front due to mixing.

where ρ is the density of air and L_V the latent heat of vaporization. $CQ = u^{*}{\cdot}C_u{\cdot}C_q$ is the turbulent exchange coefficient for moisture, that contains a thermal component, C_q, the exchange coefficient for latent heat, and a mechanical component, $u^{*}{\cdot}C_u$, where u^{*} is the friction velocity and C_u is the exchange coefficient for momentum. $\Delta q = q_S - q_a$ also contains a thermal component, where q_a the air specific humidity and q_S the saturation specific humidity corresponding to SST. Positive Q_E means the ocean heats the atmosphere and vice-versa. The sign of Q_E is set by the sign of Δq.

Figure 6 shows the co-spectrum of CQ and Δq multiplied by L_V. The lower right part of the co-spectrum (red region) indicates a positive correlation between CQ and Δq. This is consistent with an increase of surface wind speed above warm SST anomalies, and with the secondary circulation (Figure 5) bringing dry air from aloft downward over the warm SST anomalies, all leading to larger positive Δq. Thus local imprints of warm SST anomalies on the atmosphere further heat the atmosphere because of the local wind speed increase and the secondary circulation. The same reasoning can be applied to cold SST anomalies, since both CQ and SST anomalies are negative.

In contrast, the upper left part of the co-spectrum (blue region) displays a negative covariance. Large-scale SST anomalies (> 500 km) are weak (up to 0.5°C instead of up to 10°C for mesoscale anomalies), so the SST remains close to the air temperature. Upper ocean mixing by intermittent large-scale winds leads to cooler SST that becomes cooler than the air temperature and also to negative Δq anomalies.

These results indicate that fully coupling the atmosphere with the ocean leads to further amplification of the air-sea heat exchange anomalies, either at large scales or mesoscales, that already exist without the coupling. The negative part of the cospectrum should not exist in an atmospheric model forced by SST and the positive part does not exist in an ocean model forced by winds and air-sea heat fluxes since both local wind and air humidity responses are not present. Figure 6 further points to the importance of the physics involved in the APBL and the ocean mixed-layer since that physics determines the imprints of one fluid on the other.

4 Conclusions

This study has investigated the high-frequency air-sea interactions at mid-latitudes, and more precisely, how the ocean locally impacts the atmosphere and vice-versa. Large-scale SST anomalies (> 500km) have small magnitudes (up to 0.5°C at most) (Small et al., 2019). This causes the atmosphere to drive the ocean (blue region on Figure 6). In contrast, mesoscale SST anomalies (<500km), driven by baroclinic instability in the ocean interior, have large magnitudes (up to 10°C). The temperature and humidity of air masses blowing over these anomalies have no time to adjust. When a southward strong wind is blowing, submesoscale SST fronts bordering these anomalies trigger wind stress curl/divergence with large magnitudes that force a secondary circulation. This secondary circulation develops quickly, and leads to local wind intensification above warm mesoscale SST anomalies. Such local secondary circulations above warm SST anomalies further increase LHF anomalies, and cause the ocean to drive the atmosphere, as shown in the red region on Figure 6.

These results have been obtained using a new realistic global atmosphere-ocean simulation with a very high spatial resolution over a three-month period during Boreal Spring. As such, this study extends the findings from recent 2-D idealized studies that use a dry atmosphere, and further stresses the importance of resolving submesoscale features not only in the ocean but also in the atmosphere. Small-scale oceanic features at the mesoscale and submesoscale show imprint on the atmospheric circulation at these scales, which feeds back to the ocean. The contribution of the resulting local LHF anomalies to the evolution of atmospheric weather still needs to be assessed over a longer time period and in

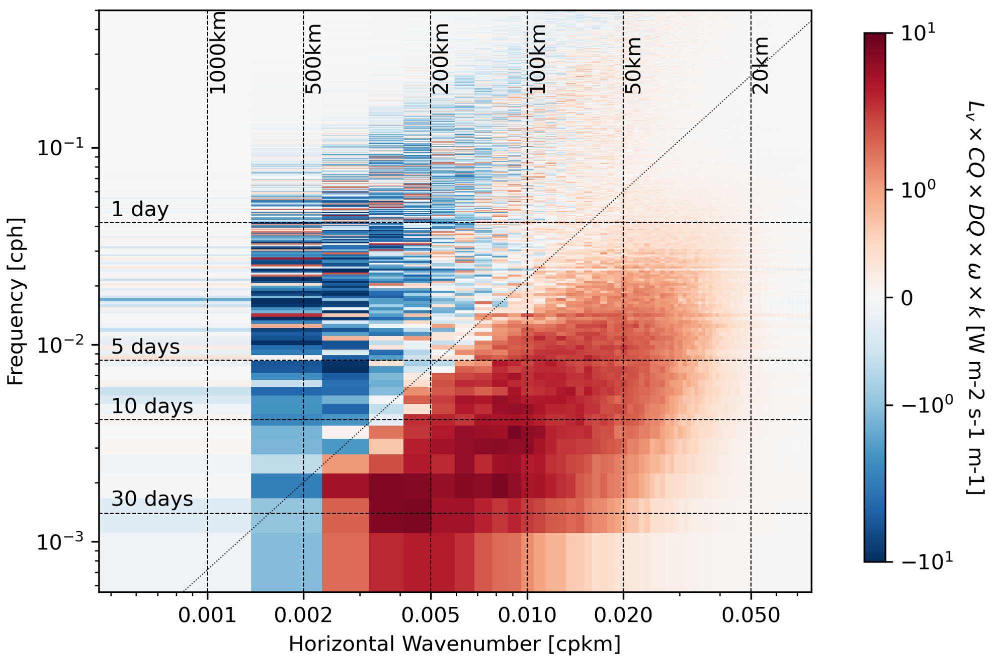

Figure 6. Co-spectrum of the latent heat fluxes. The co-spectrum is presented in a variance preserving form, which allows to directly compare the relative contribution of different time and space scales to the total covariance. See the supplementary part for the methodology to compute the co-spectrum.

the global ocean. Our global coupled simulation will be integrated for more than a year in the near future, allowing the analysis shown in this study to be conducted in different regions of the world ocean and in different seasons. Since the momentum and humidity budget terms will be available in the upcoming simulation, a momentum and humidity budget analysis will be conducted to provide more information on the mechanisms involved.

Acknowledgments

Data leading to this publication was made available as part of a Zenodo repository at: `https://zenodo.org/record/5669247/#.YYyqy71BweU`

References

Chelton, D. B., Esbensen, S. K., Schlax, M. G., Thum, N., Freilich, M. H., Wentz, F. J., … Schopf, P. S. (2001). Observations of coupling between surface wind stress and sea surface temperature in the eastern tropical pacific. *Journal of Climate*, *14*(7), 1479–1498.

Chelton, D. B., Schlax, M. G., Freilich, M. H., & Milliff, R. F. (2004). Satellite measurements reveal persistent small-scale features in ocean winds. *science*, *303*(5660), 978–983.

Chelton, D. B., Schlax, M. G., & Roger, M. S. (2011). Global observations of nonlinear mesoscale eddies. *Progress in Oceanography*, *91*(2), 167-216.

Foussard, A., Lapeyre, G., & Plougonven, R. (2019). Response of surface wind divergence to mesoscale sst anomalies under different wind conditions. *Journal of the Atmospheric Sciences*, *76*(7), 2065-2082.

Foussard, A., Lapeyre, G., & Riwal, P. (2019). Storm tracks response to oceanic eddies in idealized atmospheric simulations. *Journal of Climate,*, *32*, 445–463.

Griffies, S. M., Winton, M., Anderson, W. G., Benson, R., Delworth, T. L., Dufour, C. O., … others (2015). Impacts on ocean heat from transient mesoscale eddies in a hierarchy of climate models. *Journal of Climate*, *28*(3), 952–977.

Kilpatrick, T., Schneider, N., & Qiu, B. (2014, 02). Boundary Layer Convergence Induced by Strong Winds across a Midlatitude SST Front*. *Journal of Climate*, *27*(4), 1698-1718. doi: 10.1175/JCLI-D-13-00101.1

Klein, P., Lapeyre, G., Siegelman, L., Qiu, B., Fu, L.-L., Torres, H., … Le Gentil, S. (2019). Ocean-scale interactions from space. *Earth and Space Science*.

Lindzen, R. S., & Nigam, S. (1987). On the role of sea surface temperature gradients in forcing low-level winds and convergence in the tropics. *Journal of the Atmospheric Sciences*, *44*(17), 2418–2436.

Liu, X., Ma, X., Chang, P., Jia, Y., Fu, D., Xu, G., … Patricola, C. M. (2021). Ocean fronts and eddies force atmospheric rivers and heavy precipitation in western north america. *Nature Communications*, *12*(1), 1–10.

Ma, J., Xu, H., Dong, C., Lin, P., & Liu, Y. (2015). Atmospheric responses to oceanic eddies in the kuroshio extension region. *Journal of Geophysical Research: Atmospheres*, *120*(13), 6313–6330.

O'Neill, L. W., Chelton, D. B., & Esbensen, S. K. (2003). Observations of sst-induced perturbations of the wind stress field over the southern ocean on seasonal timescales. *Journal of Climate*, *16*(14), 2340–2354.

Putrasahan, D. A., Miller, A. J., & Seo, H. (2013). Isolating mesoscale coupled ocean–atmosphere interactions in the kuroshio extension region. *Dynamics of Atmospheres and Oceans*, *63*, 60–78.

Rackow, T., Sein, D. V., Semmler, T., Danilov, S., Koldunov, N. V., Sidorenko, D., … Jung, T. (2019). Sensitivity of deep ocean biases to horizontal resolution in prototype cmip6 simulations with awi-cm1. 0. *Geoscientific Model Development*, *12*(7), 2635–2656.

Small, R. J., Bryan, F. O., Bishop, S. P., & Tomas, R. A. (2019). Air–sea turbulent heat fluxes in climate models and observational analyses: What drives their variability? *Journal of Climate*, *32*(8), 2397–2421.

Strobach, E., Molod, A., Trayanov, A., Forget, G., Campin, J.-M., Hill, C., & Menemenlis, D. (2020). Three-to-six-day air–sea oscillation in models and observations. *Geophysical Research Letters*, *47*(10), e2019GL085837. (e2019GL085837 10.1029/2019GL085837) doi: 10.1029/2019GL085837

Su, Z., Torres, H., Klein, P., Thompson, A. F., Siegelman, L., Wang, J., ... Hill, C. (2020). High-frequency submesoscale motions enhance the upward vertical heat transport in the global ocean. *Journal of Geophysical Research: Oceans*, *125*(9), e2020JC016544.

Su, Z., Wang, J., Klein, P., Thompson, A. F., & Menemenlis, D. (2018). Ocean submesoscales as a key component of the global heat budget. *Nature communications*, *9*(1), 775.

Sullivan, P. P., McWilliams, J. C., Weil, J. C., Patton, E. G., & Fernando, H. J. (2020). Marine boundary layers above heterogeneous sst: Across-front winds. *Journal of the Atmospheric Sciences*, *77*(12), 4251–4275.

Takatama, K., & Schneider, N. (2017). The role of back pressure in the atmospheric response to surface stress induced by the kuroshio. *Journal of the Atmospheric Sciences*, *74*(2), 597–615.

Thomas, L. N., Tandon, A., & Mahadevan, A. (2008). Submesoscale processes and dynamics. *Ocean modeling in an Eddying Regime*, *177*, 17–38.

Wenegrat, J., & Arthur, R. (2018). Response of the atmospheric boundary layer to submesoscale sea surface temperature fronts. *Geophysical Research Letters*, *45*(24), 13–505.

Supporting Information for "Local Air-Sea Interactions at Ocean submesoscales in Western Boundary Current"

Ehud Strobach[1], Patrice Klein[2,3], Andrea Molod[4], Abdullah A. Fahad[4],

Atanas Trayanov[4,5], Dimitris Menemenlis[6], Hector Torres[6]

[1]Agricultural Research Organization, Rishon Lezion , Israel

[2]G.P.S. Division, California Institute of Technology, Pasadena, CA, USA

[3]Laboratoire de Météorologie dynamique, Ecole Normale Supérieure, Paris, France

[4]NASA/Goddard Space Flight Center

[5]Science Systems and Applications Inc., Greenbelt, MD, US

[6]Jet Propulsion Laboratory, California Institute of Technology, Pasadena, CA, USA

Contents of this file

S1. Frequency-wavenumber spectrum and co-spectrum

The ω-k spectrum of a given variable $\phi(x, y, t)$ is computed in the Gulf stream domain and over two month. We refer the reader to (Torres et al., 2018) for the full methodology.

However, briefly, before computing the ω-k spectrum of a $\phi(x, y, t)$, its linear trend is removed and a 3-D Hanning window is subsequently applied to the de-trended $\phi(x, y, t)$ (Qiu et al., 2018). A discrete 3-D Fourier transform is then computed to retrieve $\hat{\phi}(k, l, \omega)$, where $\hat{.}$ is the Fourier transform, k the zonal wavenumber, l the meridional wavenumber, and ω the frequency. Finally, the 3-D Fourier transform is used to compute a 2-D spectral density, $|\hat{\phi}|^2(\kappa, \omega)$ where κ is the isotropic wavenumber defined as $\kappa = \sqrt{k^2 + l^2}$. The transformation from an anisotropic spectrum to an isotropic spectrum is performed following the methodology described by (Savage et al., 2017).

ω-k co-spectra of vertical heat fluxes are computed similar to the ω-k spectrum, following the methodology described in (Flexas et al., 2019). First, the Fourier transforms of vertical velocity $\widehat{W}(k, l, \omega)$ and temperature $\widehat{T}(k, l, \omega)$ are calculated. The co-spectrum of vertical heat fluxes is then given by

$$\widehat{W.T}\,(k, l, \omega) = Re\left[\widehat{W}.\widehat{T}^*\,(k, l, \omega) + \widehat{W}^*.\widehat{T}\,(k, l, \omega)\right]$$

where Re is the real part of the complex quantity, and asterisk (*) the complex conjugate. The 2-D co-spectrum $\widehat{W.T}\,(\kappa, \omega)$ is retrieved using the same methodology as before.

The ω-k spectrum and co-spectrum are presented in a variance preserving form for easier comparaison across the frequency-wavenumber domain.

S2. SST/wind co-spectrum

Figure S1 displays the ω-k spectra of wind and SST anomalies (top panels) as well as the co-spectrum of wind and SST (bottom panel).

Wind and SST variances occupy different regions of the spectral space separated by a sloped line (dashed line on Figures S1, top panels) that follows $\omega/\omega_o \approx C_{nd}.[k/k_o]^{1.5}$ (with $\omega_o = 2.10^{-3} hour^{-1}$, $k_o = 2.10^{-3} km^{-1}$, $C_{nd} \sim 20$). Winds have principally larger spatial scales and smaller time scales than SST: Wind variance is large at periods of one day and length scales of 300–500km whereas SST variance is large at smaller space scales (100–300 km) and larger periods (10–30days). Furthermore, the wind and SST variances are each distributed along a line $\omega \approx C.k$ where $C = C_{wind} = 3.5m/s$ for the wind variance (Figure S1, top left panel) and $C = C_{SST} = 14cm/s$ for the SST variance (Figure S1, top right panel). These distributions can be interpreted in terms of the Taylor hypothesis that relates temporal and spatial fluctuations through a characteristic velocity (Gill, 1982). Values of C_{wind} and C_{SST} respectively match the root mean square (RMS) of atmosphere and ocean velocities in the GS region (Torres et al., 2018). Note that SST variance is intimately associated with the mesoscale kinetic energy since the KE spectrum (not shown) is found in the same spectral region as SST anomalies. Similarly, the air temperature and humidity variance share the same spectral characteristics (not shown) as for the wind variance.

The co-spectrum of wind and SST (Figure S1, bottom panel) reveals a negative covariance above the dashed line and positive below. A negative covariance indicates that wind anomalies are not driven by SST anomalies in this spectral range where wind variance is large and SST variance weak (Figure S1, top panels). Rather large-scale wind anomalies with periods of some hours up to a few days are driven by the intrinsic atmospheric variability (Small et al., 2019, 2020), such as those associated with the cold-dry air outbreaks mentioned before. As a result, winds cool the ocean at these scales. A positive covariance below the dashed line indicates that wind anomalies are driven by SST anomalies. Actually, wind anomalies in this region are much smaller (Figure S1, top left panel). SST anomalies in this region have a much larger magnitude (Figure S1, top right panel) and are driven by the intrinsic ocean variability. Such result, in terms of covariance sign change, is reported in Small et al. (2019) for monthly time scale. They found that the spatial scale for which the covariance changes its sign is ∼600 km (from their Figure 13), a value a little larger than the one found in our study (see Figure S1, bottom panel).

References

Flexas, M. M., Thompson, A. F., Torres, H. S., Klein, P., Farrar, J. T., Zhang, H., & Menemenlis, D. (2019). Global estimates of the energy transfer from the wind to the ocean, with emphasis on near-inertial oscillations. *Journal of Geophysical Research: Oceans*.

Gill, A. E. (1982). Atmosphere. *Ocean dynamics*, *30*, 662.

Qiu, B., Chen, S., Klein, P., Wang, J., Torres, H., Fu, L.-L., & Menemenlis, D. (2018). Seasonality in transition scale from balanced to unbalanced motions in the world ocean. *Journal of Physical Oceanography*, *48*(3), 591–605.

Savage, A. C., Arbic, B. K., Richman, J. G., Shriver, J. F., Alford, M. H., Buijsman, M. C., ... others (2017). Frequency content of sea surface height variability from internal gravity waves to mesoscale eddies. *Journal of Geophysical Research: Oceans*, *122*(3), 2519–2538.

Small, R. J., Bryan, F. O., Bishop, S. P., Larson, S., & Tomas, R. A. (2020). What drives upper-ocean temperature variability in coupled climate models and observations? *Journal of Climate*, *33*(2), 577–596.

Small, R. J., Bryan, F. O., Bishop, S. P., & Tomas, R. A. (2019). Air–sea turbulent heat fluxes in climate models and observational analyses: What drives their variability? *Journal of Climate*, *32*(8), 2397–2421.

Torres, H. S., Klein, P., Menemenlis, D., Qiu, B., Su, Z., Wang, J., . . . Fu, L.-L. (2018). Partitioning ocean motions into balanced motions and internal gravity waves: A modeling study in anticipation of future space missions. *Journal of Geophysical Research: Oceans*, *123*(11), 8084–8105.

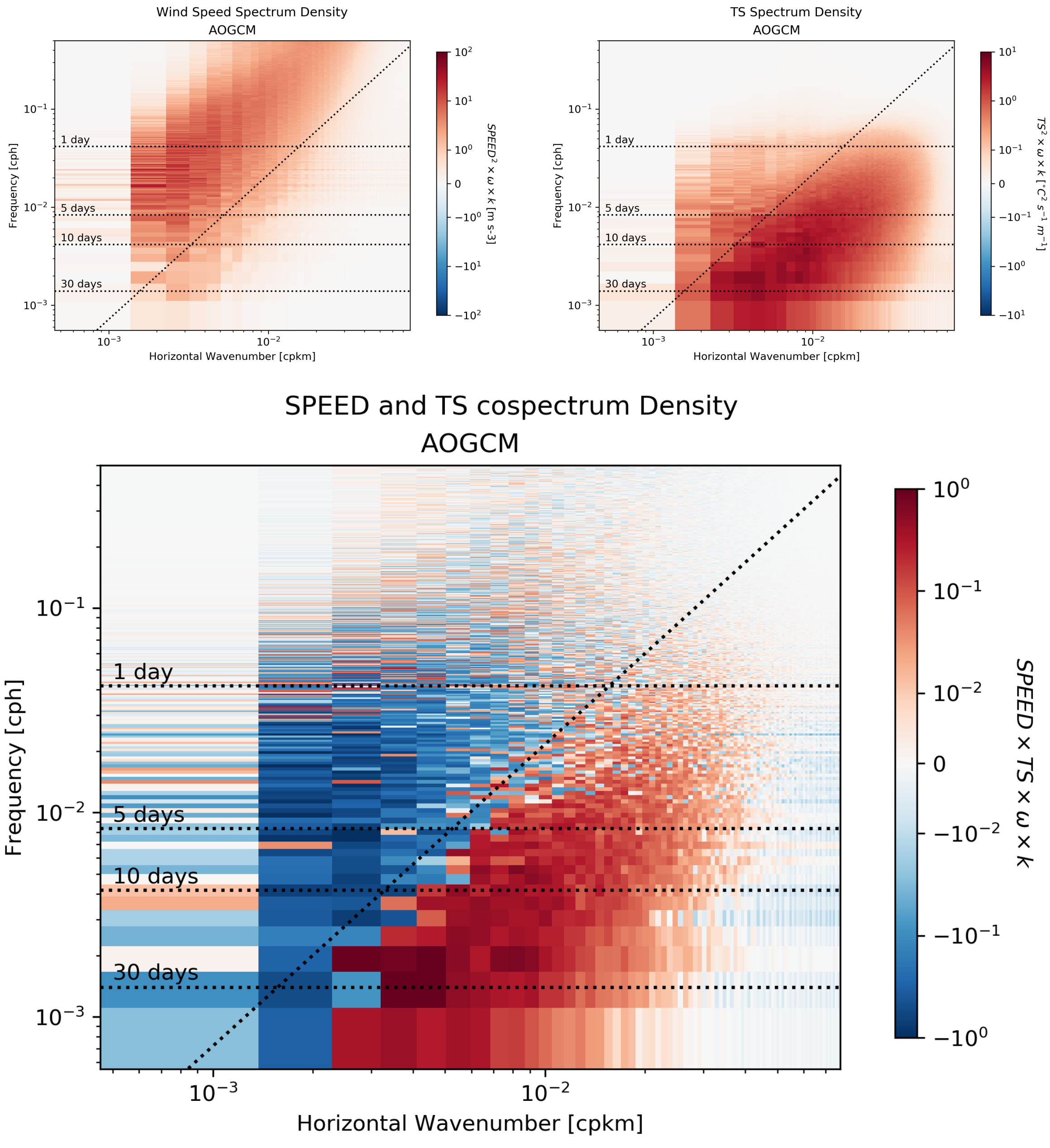

Figure S1. ω-k spectrum of the wind speed (top left panel), SST (top right panel) and ω-k co-spectrum of wind and SST (bottom panel).